Growth Behavior of Oxide Forming on a Sputtered Oxygen-Enriched Type 304 Stainless Steel

L. Zhou, D.G. Lees, R.D. Arnell, D. Johnson, and A. Chew

Type 304 stainless steel was deposited with and without added oxygen and then oxidized at 900 °C in 0.1 atm oxygen. The oxidation rate of the oxygen-enriched steel was lower than that of the steel without added oxygen, and the oxide adhesion was better. Line scans on cross-sectioned scale on the oxygen-enriched steel showed that inward oxygen diffusion had occurred; however, this was not shown by any of the line scans on the steel without added oxygen. The diffusion rate of cations through chromia scale was reduced by the oxygen enrichment. A secondary ion mass microscopy study showed that sulfur segregation to the oxide scale occurred during oxidation. The extent of this segregation for the oxygen-enriched steel was much lower than that for the steel without added oxygen. The results are explained in terms of the sulfur effect theory by postulating that impurity sulfur segregated to oxide particles in the oxygen-enriched steel, resulting in a reduced sulfur level in the scale and at the oxide/metal interface.

Keywords
oxidation, chromia, sulfur

1. Introduction

OXIDATION resistance of a metal depends on both penetration resistance and adhesion of the oxide scale forming on the metal. Most of the alloys for high-temperature oxidation resistance are either chromia formers or alumina formers, because chromia and alumina can provide good protection against further oxidation. Chromia is especially resistant to sulfur attack. In recent years, it has been found that impurity sulfur plays an important role in the adhesion of alumina and chromia scales (Ref 1-3). Lees further proposed that sulfur also affects the cation diffusion rate in chromia scale (Ref 3). Both effects have been combined in what we call the sulfur effect theory (Ref 3,4), which is summarized below.

During oxidation of a metal, impurity sulfur in the metal segregates to the oxide/metal interface and dissolves in the oxide scale. The sulfur at the oxide/metal interface decreases the oxide scale adhesion, and the sulfur in the scale promotes cation diffusion transport through the scale.

One of the most important steps in the development of oxidation-resistant alloys over the past 30 years has been the use of reactive elements such as yttrium, cerium, and hafnium as alloying additives. These elements remarkably improve the adhesion of chromia and alumina scales and reduce the cation diffusion rate in chromia, resulting in a decreased oxidation rate (Ref 5, 6). Lees has proposed that this is simply because impurity sulfur in metals is combined with or absorbed by the reactive elements and is thus prevented from segregating to the scale/metal interface and from dissolving in the scale (Ref 3).

L. Zhou, Ghulam Ishaq Khan Institute of Engineering Science & Technology, Topi, N.W.F.P., Pakistan; **D.G. Lees,** Manchester Materials Science Centre, University of Manchester and UMIST, Manchester M1 7HS, U.K.; **R.D. Arnell,** University of Salford, Salford M5 4WT, U.K.; **D. Johnson,** Centre for Surface and Materials Analysis Ltd., Armstrong House, Manchester M1 7ED, U.K.; **A. Chew,** Loughborough University of Technology, Loughborough, LE11 3TU U.K.

However, in most of the previous proposals (Ref 5, 6), various possible chemical effects of the reactive elements were suggested to be responsible for their beneficial effects on oxidation resistance.

The present investigation was carried out to test the theory directly by studying the chromia scale that had been made adherent without addition of a reactive element. The work is based on the results of Zhou et al. (Ref 7), which showed that addition of oxygen to a sputtered cobalt-chromium alloy greatly improved oxide adhesion. In the present work, we prepared sputter-deposited layers of type 304 stainless steel with and without added oxygen and compared the oxidation behavior and in particular the growth mechanism of the chromia scale.

2. Experimental Procedure

2.1 *Sputtering and the Sputter-Deposited Materials*

The materials for this study were made by sputter deposition with a direct-current magnetron sputtering system. The sputtering target was made of commercial type 304 stainless steel. The substrates, 10×8 mm^2 in size, were cut from 0.5 mm thick cold-rolled type 304 stainless steel sheet. Oxygen-enriched steel was produced by sputtering with a controlled flow of oxygen into the sputtering chamber. For comparison, a similarly sputtered reference steel without oxygen addition was prepared. The deposition rate was approximately 2 μm/h. The thickness of the sputtered layers was approximately 25 μm. The compositions of both sputtered steels were very close and were typical of a commercial type 304 stainless steel (Table 1).

2.2 *Isothermal Oxidation Tests*

Isothermal oxidation runs were carried out at 900 °C in pure oxygen at 0.1 atm pressure in a manometric apparatus, which has been described in Ref 4.

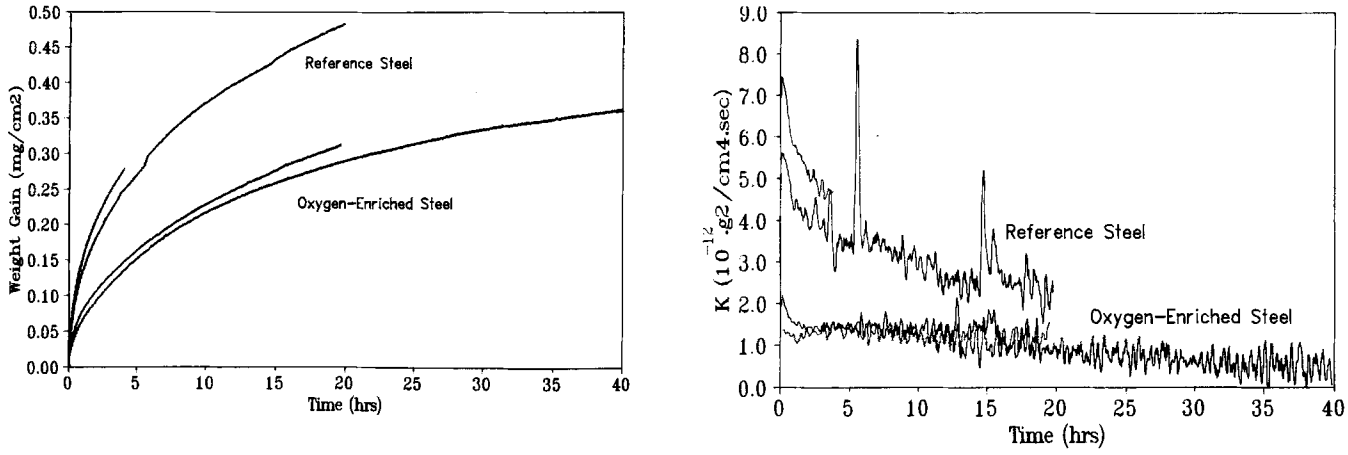

(a) (b)

Fig. 1 Oxidation kinetics of the sputtered type 304 stainless steels at 900 °C, 0.1 atm oxygen. (a) Weight gain versus time. (b) Instantaneous parabolic rate constant

Table 1 Chemical composition of sputter-deposited type 304 stainless steels

Material	Composition, wt % Cr	Ni	Mn	Si	Fe
Oxygen-enriched steel	19.33	9.74	1.62	0.41	bal
Reference steel	19.28	8.83	1.67	0.45	bal

2.3 *Two-Stage Oxidation and SIMS/SIMM Microanalyses*

A specimen of the reference steel and a specimen of the oxygen-enriched steel were oxidized together in the manometric apparatus at 900 °C for 24 h in natural oxygen and, at the same temperature, a further 76 h in oxygen enriched in $^{18}O_2$. The gas change took less than 3 min. At the end of the oxidation run, the $^{18}O_2$ was pumped out of the furnace before the specimens were removed from the hot zone in order to minimize the possibility of gas penetration along possible cooling-induced fissures in the scale.

The two-stage oxidized specimens were cross-sectioned, and the distributions of ^{18}O and ^{16}O in the scale were determined by means of imaging secondary ion mass spectroscopy (SIMS). A primary beam of 10 keV, 0.5 nA Ga^+ ions with a minimum diameter of less than 0.5 μm was used, and the secondary ions were analyzed by means of a quadrupole mass spectrometer.

The distributions of sulfur and chromium in the cross-sectioned scales and in the underlying sputtered layers were determined by secondary ion mass microscopy (SIMM). The microscope used for SIMM is an ion analog of the transmission electron microscope. In this case, the primary ion beam acts as a source of illumination, and the ion image is formed using ion lenses to maintain the spatial distribution of the secondary ions as they are transmitted through the mass spectrometer. The secondary ion image is then formed by the impact of the spatially distributed secondary ions on a screen. By setting the mass spectrometer for transmission of the ions of a certain mass, which corresponds to a certain element or a certain group of elements, a real-time display of the element distribution can be produced.

The present study was carried out on a Cameca IMS 3f system. A primary beam of 10 keV, 0.1 μA Cs^+ ions with a diameter of about 200 μm was used, and the secondary ions were analyzed by means of a magnetic sector spectrometer, which has a resolution greater than 0.1 dalton and is able to distinguish small differences, such as that of ^{32}S from a cluster of two ^{16}O. In this system, the spatially distributed intensity of ion emission can also be digitally recorded and used to remap the distribution.

3. Results

3.1 *Oxidation Kinetics*

The weight-gain curves are plotted in Fig. 1(a) and the corresponding instantaneous parabolic rate constants ($K = 2w \cdot dw/dt$) in Fig. 1(b). X-ray diffractometry showed that the oxide scales formed on both steels consisted of an inner layer of chromia and an outer layer of spinel $Mn_{1.5}Cr_{1.5}O_4$. The thicknesses of the oxide layers on the specimens oxidized for 100 h are listed in Table 2.

3.2 *Morphology of the Oxide Scales*

The scale formed on the oxygen-enriched steel after 100 h of exposure at 900 °C adhered quite well, even though the sputtered layer of the steel was convoluted (Fig. 2a). Only a few fissures appeared on some ridges of the convoluted surface. At the

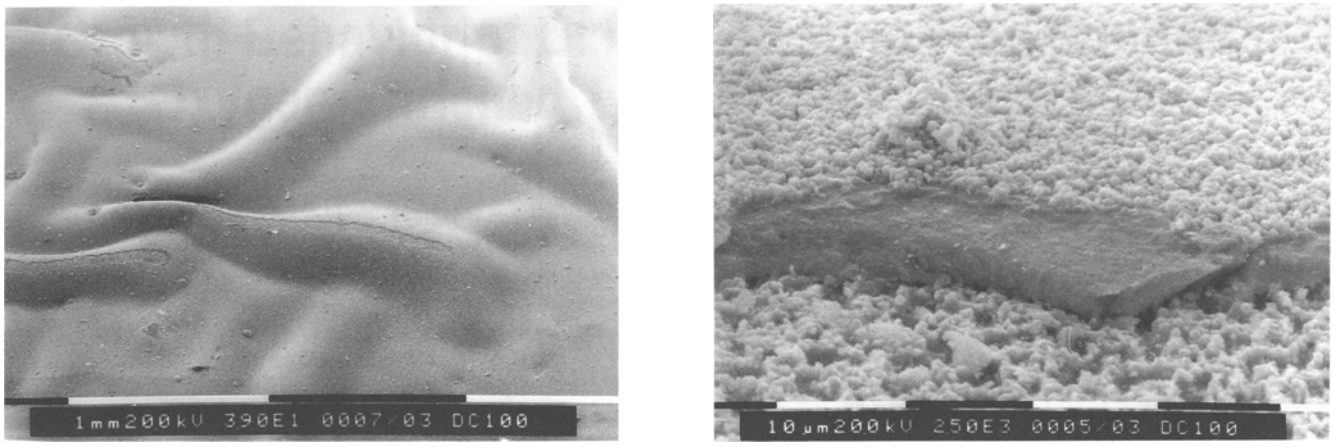

(a) (b)

Fig. 2 Oxide scale on the oxygen-enriched steel, oxidized for 100 h at 900 °C (24 h in $^{16}O_2$ and 76 h in $^{18}O_2$ enriched oxygen). The sputtered steel layer became convoluted during oxidation, and the oxide scale has followed the convolutions. (a) Convolution of the sputtered

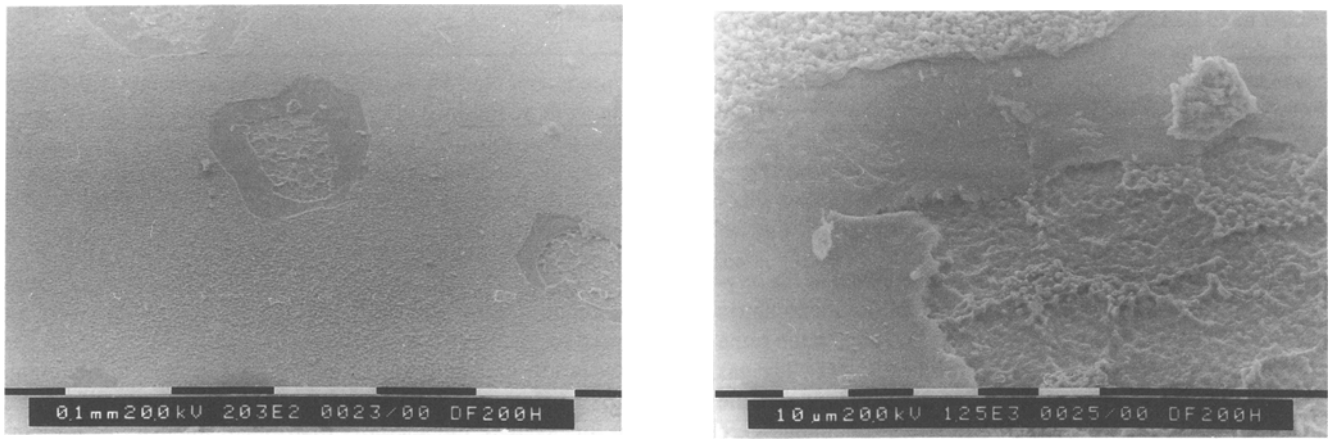

(a) (b)

Fig. 3 (a) Spotlike spallation of the scale on the oxidized reference steel. (b) Higher-magnification view of (a)

Tabld 2 Thickness of the oxide layers on sputtered type 304 stainless steels(a)

Material	Oxide thickness, µm		
	Inner layer	Outer layer	Total scale
Reference steel	4.0	4.7	8.7
Oxygen-enriched steel	2.9	1.2	4.1

(a) Oxidized for 100 h at 900 °C

fissure, the two-layer structure of the scale was revealed clearly (Fig. 2b). The sputtered layer of the reference steel was not convoluted, but some spotlike spallation occurred (Fig. 3).

Cross sections of the specimens are shown in Fig. 4. Cavities were visible at the scale/metal interface of the reference steel, but none could be seen at the oxide/metal interface of the oxygen-enriched steel. The oxide protrusions along the scale/metal interface of the oxygen-enriched steel were shown by energy-dispersive x-ray analysis (EDAX) to be of the same composition as the inner chromia layer (Fig. 5a).

Particles sized from 0.5 to 2.0 µm were found in the oxygen-enriched steel but not in the reference steel (Fig. 4). Analysis by EDAX showed that they were enriched in silicon (Fig. 5b). As silicon is the most reactive element in this steel, it is reasonable to suppose that particles of silica were present.

3.3 *Distribution of Oxygen-18 in the Scales*

Typical SIMS line scans for ^{18}O and ^{16}O distributions across the scales are plotted in Fig. 6. The positions of ^{18}O peaks in relation to ^{16}O peaks show that the scales on both specimens grew primarily by cation diffusion. The slopes of the ^{18}O profiles

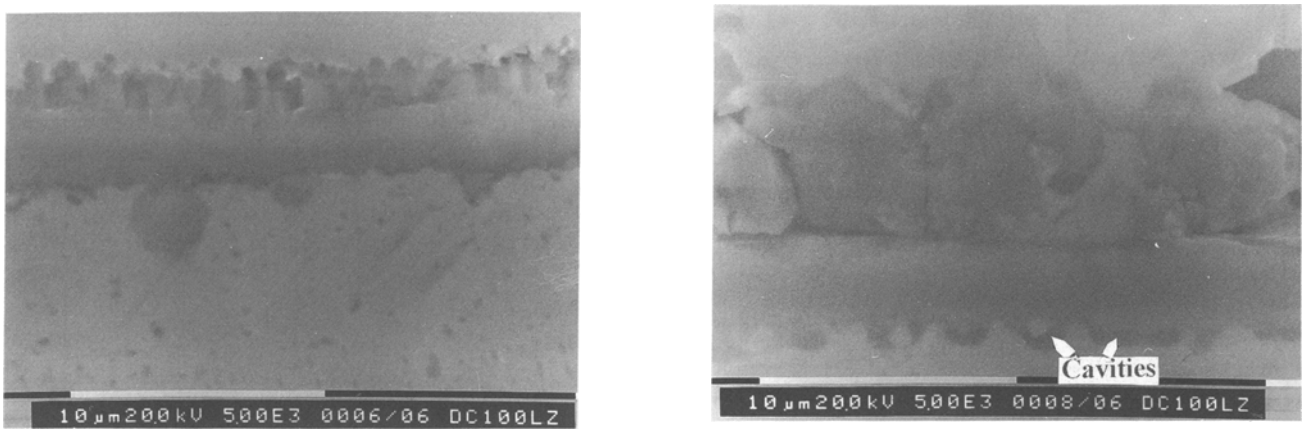

(a) (b)

Fig. 4 Cross sections of the specimens, oxidized for 100 h at 900 °C (24 h in $^{16}O_2$ and 76 h in $^{18}O_2$ enriched oxygen). (a) Oxygen-enriched steel. (b) Reference steel

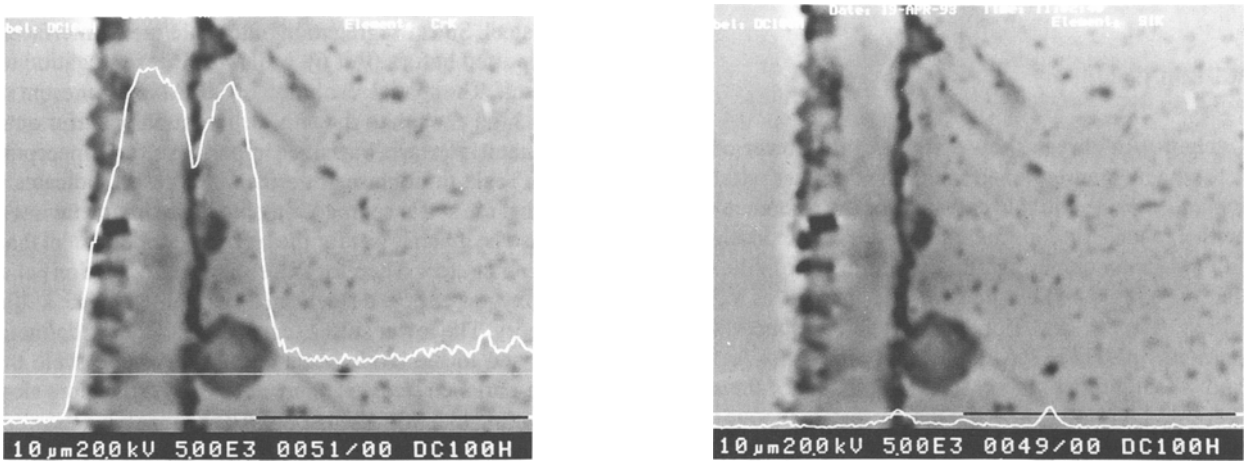

(a) (b)

Fig. 5 Line scan profiles produced by EDAX on the cross section shown in Fig. 4(a). (a) Cr K_α. (b) Si K_α. The position of the scan is shown in (a).

Table 3 Ratios of sulfur count rate to chromium count rate in scale (S/Cr) and sulfur count rate in oxide scale to that in substrate metal (S/S_m)

Material	Ratio S/Cr	Ratio S/S_m
Oxygen-enriched steel	0.0092	1.3
Reference steel	0.081	6.0

from their peaks toward the oxide/metal interfaces show that in the oxygen-enriched steel, some oxygen diffusion occurred, whereas in the reference steel none occurred.

3.4 *Distribution of Sulfur*

The distributions of sulfur examined by SIMM were originally displayed in the form of color-contour maps. It was revealed that the scales on both steels contained more sulfur than the sputtered metals on which they were formed. For the oxygen-enriched steel, however, the increase of sulfur in the scale was much lower than in the reference steel. Table 3 gives the sulfur-to-chromium ratio in the scale and the sulfur increase ratio for both steels. These data were obtained by comparing the colors on the maps with those on a reference scale. This method involves some error, but the average of several calculations showed a sulfur content in the scale on the oxygen-enriched

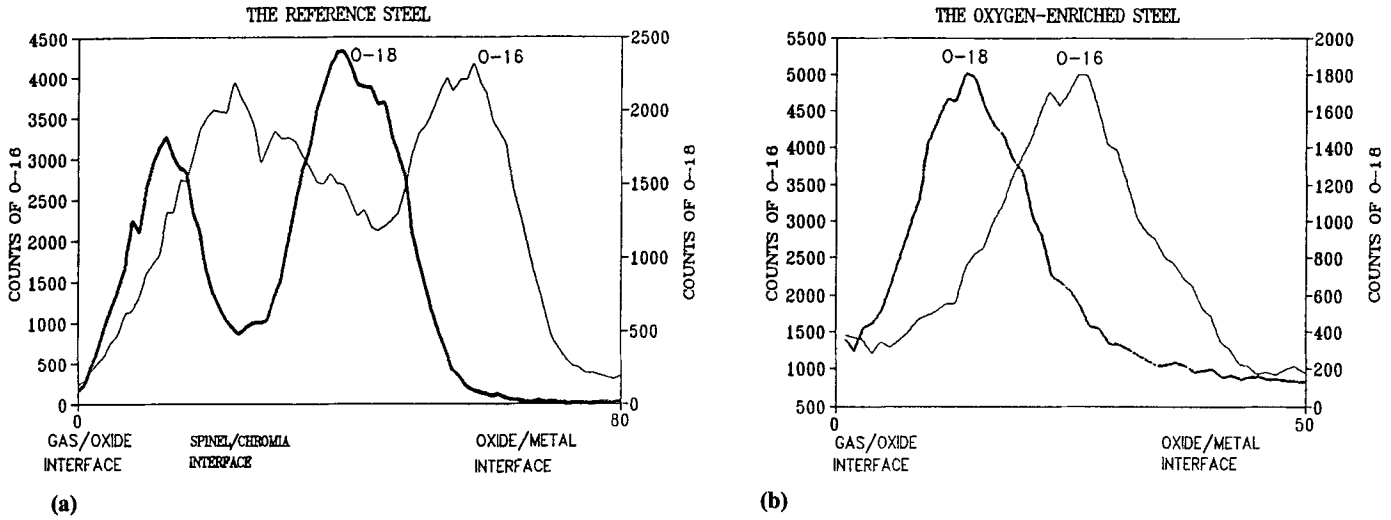

Fig. 6 Line scans produced by SIMS across the oxide scales of the specimens oxidized for 100 h at 900 °C (24 h in $^{16}O_2$ and 76 h in $^{18}O_2$ enriched oxygen). (a) Oxygen-enriched steel. (b) Reference steel

steel one-tenth that of the scale on the reference steel. This is well outside the limits of error.

4. Discussion

The weight-gain curves show a significantly lower oxidation rate for the oxygen-enriched steel. The decrease with time of instantaneous parabolic rate constant for the reference steel agrees with a repeatedly reported fact that during oxidation of this kind of silicon-containing alloy, a thin layer of silica between the oxide scale and the metal forms and acts as a diffusion barrier (Ref 8, 9). For the oxygen-enriched steel, silicon-enriched particles (presumably of silica) are formed, leaving no silicon or less silicon for development of the silica layer. Therefore, it is not surprising that its instantaneous parabolic constant did not decrease so remarkably during oxidation.

The outer spinel layer on the reference steel was much thicker than that on the oxygen-enriched steel, and the spinel/chromia thickness ratio was much greater even though the chromia scale was thicker. This suggests that cation diffusion through the chromia layer on this steel was faster than in the chromia on the oxygen-enriched steel, because the outer layer grows by cation diffusion through the inner chromia scale. In oxidation of metals, the outward cation diffusion and inward oxygen diffusion compete with each other. The higher the cation diffusion rate, the less the opportunity for oxygen to diffuse inward, since cations can react with atoms of oxygen right at the surface. Therefore, the ^{18}O tracer analysis results also suggest a higher cation diffusion rate for the reference steel. Cavities were observed at the scale/metal interface of the reference steel but not at this interface on the oxygen-enriched steel. This agrees with a higher ratio of cation diffusion in the reference steel; outward cation diffusion causes a vacancy injection onto the scale/metal interface (Ref 5). The topography of the oxidized samples clearly demonstrates that oxide scale adhesion was much improved by oxygen enrichment.

Study by SIMM revealed that sulfur segregation to the oxide scale took place during oxidation. The extent of the segregation was much lower for the oxygen-enriched steel than for the reference steel. Sulfur segregation onto scale/metal interfaces has been reported before (Ref 6), but not sulfur segregation to the scale itself. The spatial resolution of SIMM in the present study was not high enough to show the segregation of sulfur onto the oxide/metal interface, but, since impurity sulfur is incorporated into the scale through the interface, this result indicates indirectly that the sulfur segregation onto the oxide/metal interface must also be much lower for the oxygen-enriched steel than for the reference steel. Therefore, the improved oxidation behavior of the oxygen-enriched steel can be explained by the sulfur effect theory. The lower sulfur segregation to the oxide/metal interface and to the oxide scale caused the oxide scale on the oxygen-enriched steel to adhere better and grow more slowly.

Scanning electron microscopy/EDAX analysis showed that during oxidation the oxygen-enriched steel was actually dispersed with particles, presumably of silica. We propose that impurity sulfur segregated to the particle/metal interfaces as well as to the scale/metal interface because both are oxide/metal interfaces. Most of the impurity sulfur is thus prevented from segregating to the scale/metal interface and from dissolving in the scale.

5. Conclusion

The results from this investigation show that oxygen enrichment reduced the cation diffusion rate in the chromia scales forming on sputtered type 304 stainless steel and improved scale adhesion. The segregation of impurity sulfur to oxide scale occurred during oxidation. The extent of this segregation in the oxygen-enriched steel was much lower than in the steel without oxygen addition. The beneficial effects of oxygen enrichment on oxide growth behavior are explained in terms of the sulfur effect theory, which states that sulfur in chromia scale

increases the cation diffusion rate and the sulfur segregates to the scale/metal interface and decreases scale adhesion.

Acknowledgments

We wish to thank the K.C. Wong Foundation for a grant via The Royal Society to one of the authors (L.Z.). which enabled this work to be carried out at Manchester Materials Science Centre. We greatly appreciate the assistance of Mr. Robin Bates of University of Salford in the preparation of the sputtered specimens.

References

1. Y. Ikeda, K. Nii and K.Yoshihara, *Trans. Jap. Inst. Met.,* Vol 24 (suppl.), 1993, p.207
2. J.G. Smeggil, *Metall. Trans.*, Vol 17A, 1986, p 923
3. D.G. Lees, *Oxid. Met.*, Vol 27, 1987, p 7
4. P. Fox, D.G.Lees, and G.W. Lorimer, *Oxid. Met.*, Vol 36, 1991, p 491
5. D.P. Whittle and J. Stringer, *Philos. Trans. R. Soc. (London) A*, Vol A295, 1980, p 309
6. J. Stringer, *Mater. Sci. Eng.*, Vol A120, 1989, p 129
7. L.Zhou, Y. Ruizeng, Z. Shouhua, and G. Liang, *Corros. Sci.*, Vol 32, 1991, p 337
8. M.J. Bennett, J.A. Desport, and P.A. Labun, *Proc. R. Soc. (London) A*, Vol A412, 1987, p 223
9. R.C. Lobb, J.A. Sasse, and H.E. Evans, *Mater. Sci. Technol.*, Vol 5, 1989, p 828